Publ. Astron. Soc. Japan (2014) 66 (SP1), S13 (1–11)
doi: 10.1093/pasj/psu087
Advance Access Publication Date: 2014 November 13

Possible signature of Alfvén wave dissipation in the localized magnetic funnels of the equatorial solar corona

Bhola N. Dwivedi,* Abhishek Kumar Srivastava, and Anita Mohan

Department of Physics, Indian Institute of Technology (Banaras Hindu University), Varanasi, Pin-221005, India

*E-mail: bnd.app@iitbhu.ac.in

Received 2014 February 13; Accepted 2014 May 8

Abstract

We analyse the Hinode/EIS 2″-spectroscopic scan data containing the spectral line formed at typical inner coronal temperature. The strong Fe XII 195.120 Å line shows the existence of funnel-like expanding flux-tubes which exhibit the signature of blue-/red-shifted plasma motions in the off-limb equatorial corona. These coronal funnels expand in the form of open magnetic field channels up to inner coronal heights. They are most likely the parts of large-scale and closed magnetic fields (loops) which exist at higher heights in the diffused equatorial corona. We also find the signature of decreasing line-widths with altitude in observed coronal funnels (e.g., funnel 1), which is the lower part of a curved loop system. This provides the most likely signature of Alfvén wave dissipation in lower part of this loop system. We also examine the blue-shifted and diffused coronal loop boundary and interfaced region (funnel 3) which shows increasing Fe XII 195.120 Å line-width along it. Therefore, it exhibits the most likely signature of Alfvén wave growth in this region which is slightly curved and rising higher in the corona. Density measurements in these funnels show that it falls off with height, but more rapidly in the second funnel. We conjecture the almost constant line-width trend as a most likely signature of Alfvén wave dissipation in this density-stratified second coronal funnel, which is also the lower part of a large-scale closed loop system. Both dissipative and growing Alfvén waves can change the non-thermal component and thus the full width at half-maximum of the Fe XII 195.120 Å line. We find the clues of Alfvén wave dissipation along the expanding field lines of the coronal funnel (lower parts of the loop system) imparting its energy to the outflowing plasma and thereby contributing to the formation of the nascent solar wind in the inner corona.

Key words: magnetic fields — magnetohydrodynamics (MHD) — Sun: corona — Sun: oscillations — Sun: UV radiation

1 Introduction

The equatorial corona, in all likelihood, is the source of large-scale but slow-speed solar wind (Habbal et al. 1997; Sakao et al. 2007). However, the problem of what energy sources power the nascent slow solar wind stream in the equatorial inner corona remains unsettled. Several studies suggest the role of Alfvén waves under the regime of magnetohydrodynamics (MHD) in heating and accelerating the

wind in the inner solar atmosphere, while ion cyclotron waves at kinetic scales in the outer solar atmosphere (e.g., Ofman & Davila 1995; Tu & Marsch 1997; Suzuki & Inutsuka 2005; Srivastava & Dwivedi 2007; Jian et al. 2009; Chmielewski et al. 2013, and references cited therein).

Accordingly, it calls for a compelling ground of debate as to how the Alfvén waves leave the signature of their presence in the solar corona. As far as the equatorial corona is concerned, Harrison, Hood, and Pike (2002) have detected the presence of such waves using the spectroscopic observations from the Solar and Heliospheric Observatory (SOHO)/Coronal Diagnostic Spectrometer (CDS) in terms of the line-width reduction with height, and found that these waves can be dissipated in the large-scale loops of the equatorial corona. Therefore, such waves may provide their energy to heat the nascent solar wind and facilitate their formation. However, Wilhelm et al. (2005) could not find any further clues to the wave activity as they could not find any significant line-width variations of the various lines observed by Solar Ultraviolet Measurements of Emitted Radiation (SUMER) and CDS in the equatorial corona. Tu et al. (2005) have reported the formation of fast solar wind in the coronal funnels locally in the polar corona. Marsch et al. (2006) have further explored such funnels in the entire quiet-Sun, linking the mass supply from chromosphere to the corona. The open expanding arches, mimicking coronal funnels at the boundary of active regions (ARs), have been suggested as the source region of the slow solar wind at diverse spatio-temporal scales (Harra et al. 2008; Subramanian et al. 2010).

The drivers of such mass supply contributing to the wind formation can be broadly categorized as magnetic reconnection or MHD wave heating, or both. Recently, Bradshaw, Aulanier, and Del Zanna (2011) have found that interchange reconnection takes place at high altitude coronal null points. This reconnection generates the rarefaction wave and exhibits the outflows observed as blueshifts in coronal emission lines at the boundaries between open and closed magnetic field regions. Tripathi et al. (2012) have also found the signature of blue- and red-shifts in the coronal loop systems. Srivastava et al. (2014) have found that the thermal heating at the footpoints of such coronal funnels can also generate the slow and sub-sonic outflows up to the inner corona that may partially contribute to the formation of the slow solar wind. McIntosh et al. (2012) and Tian et al. (2013) have found the presence of Alfvén waves in the chromospheric spicule related flows and large-scale coronal AR outflowing regions, respectively. These structures have revealed that such transverse waves can power the localized plasma flows, contributing to the nascent wind formation.

In the present work, we detect the presence of the localized coronal funnels in the equatorial corona from where the plasma blue-shift and red-shift are observed. The line-width decrement of Fe XII 195.12 Å with height is also evident in these coronal funnels, which are the lower parts of the curved loops. We suggest the line-width decrement to be associated with the reduction of the non-thermal component associated with the formation of the particular line (in the present case Fe XII 195.12 Å; constant line formation temperature $T_f = 1.2$ MK). This is attributed to the presence of dissipative Alfvén waves.

In section 2, we describe the details of the observation and data reduction. Results and discussion are presented in section 3.

2 Observation and data reduction

The Extreme Ultraviolet Imaging Spectrometer (EIS) onboard the Hinode spacecraft is a normal-incidence extreme ultraviolet (EUV) spectrometer (Culhane et al. 2006). Hinode/EIS provides both high spectral resolution (i.e., 0.0223 Å) and high spatial resolution (i.e., $\sim 1''$) per pixel spectroscpic and imaging observations of the localized coronal plasma and its dynamics. It observes high-resolution spectra in short-wavelength band (170–211 Å) and long-wavelength band (246–292 Å). The EIS is the imaging spectrometer of which $40''$ and $266''$ slots are used for the image analyses using the light curves and emissions per pixel, while the $1''$ and $2''$ slits are utilized for spectral and Doppler analyses using spectral-line profiles. It observes in two modes: (i) scan; (ii) sit and stare. An equatorial coronal observation recorded on 2007 February 7 has been used in this present work.

The analysed observations were taken on 2007 February 7 and the data-set contains spectra of various lines formed at chromospheric, transition region (TR), and coronal temperatures. The scanning observation started at 16:51:00 UT on 2007 February 7. The scanning steps (various exposures) do not have any off-set due to spacecraft jitters in the field-of-view containing the off-limb region of our interest. The selected first funnel, which is the lower part of southmost loop and its boundary in AR 10940 [cf. SOHO/EIT image in figure 1; reference coordinates near its footpoint: ($950''.96$, $-180''.90$)] exhibits the blue-shift. The open and expanding second funnel, which is the lower part of a curved loop system in the active region, exhibits the red-shift. The reference coordinates of this funnel near its footpoint is ($972''.92$, $-91''.90$). Lastly we select a blue-shifted boundary of an active region loop that is higher, and most likely associated with the open magnetic field channel of an active region boundary opening at still higher heights in the corona. The reference coordinates of this funnel

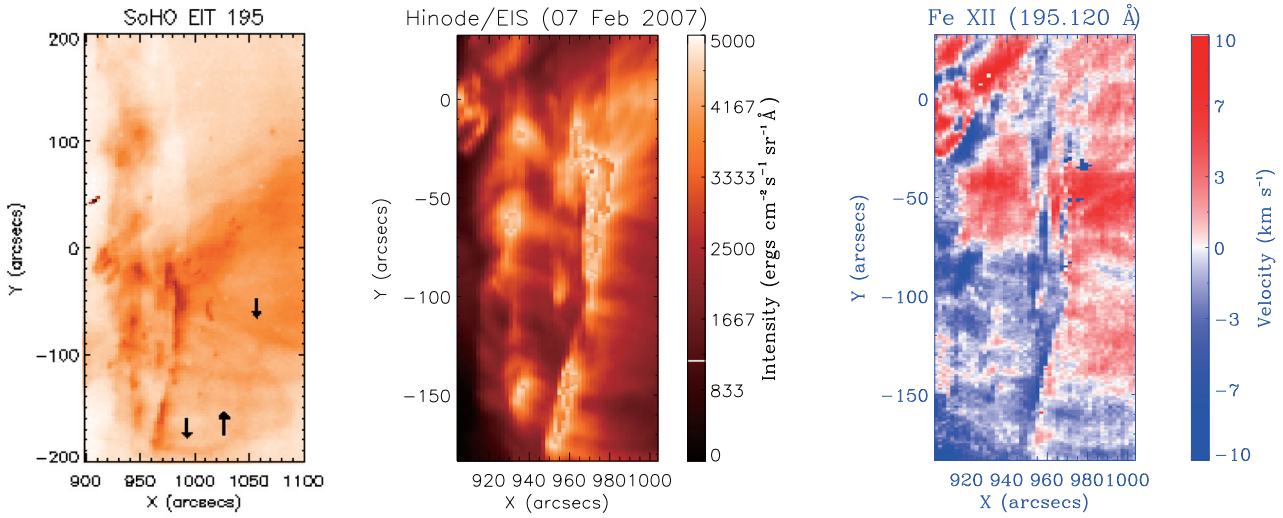

Fig. 1. Left-hand panel: negative color image of Fe XII 195.12 Å, taken by the SOHO/EIT on 2007 February 7, shows the larger field-of-view of western equatorial corona. Middle panel: intensity map of Fe XII 195.120 Å, observed by Hinode/EIS on 2007 February 7, represents the western equatorial corona. Right-hand panel: velocity map of Fe XII 195.120 Å displays the blue- and red-shifted lower parts of various loops and their boundaries. (Color online)

near its footpoint is (966″.93, −162″.90). However, the observations of the red-/blue-shift in the off-limb equatorial corona also depend on the orientation of these tubes.

We apply the standard EIS data-reduction procedures and calibration files/routines to the data obtained at the EUV-telescope which is the raw, i.e., zeroth-level data. The subroutines can be found in the sswidl software tree working under the Interactive Data Language (IDL) environment. These standard subroutines reduce for dark-current subtraction, cosmic-ray removal, flat-field correction, hot pixels, warm pixels, and bad/missing pixels. The data are saved in the level-1 data file, while associated errors are saved in the error file.

3 Results and discussion

We fit the double Gaussian on the clean line of Fe XII 195.12 Å, and derive the intensity, Doppler velocity, and full width at half-maximum (FWHM) maps of the observed western equatorial corona (Young et al. 2009; software Note 17 of Hinode/EIS). The single Gaussian fitting may not be appropriate for the Fe XII 195.12 Å line in an active and denser regions where the blending of Fe XII 195.118 Å line may affect its line-profile. However, it is not true in all the cases as it depends on the relative contribution of the blend. The present blended line is a weak density-sensitive line and becomes effective only in the case of high-density evolution in the active regions. In our observations, we fit the data using a double Gaussian, implementing the method developed by Young et al. (2009). We constrain the Fe XII 195.120 Å weakly blended line by Fe XII 195.118 Å within the range of ±60 mÅ from its centroid with its effective maximum contribution up to 28% of the peak intensity of Fe XII 195.12 Å line. By searching the possible intensity in a given threshold at each pixel (it is a freely chosen parameter here), we perform the double Gaussian fit to remove any possible effect of blending. It is to be noted that the contribution of the blend is weak because its average contribution in our data is around 6%, even at the locations near the footpoints of the selected funnels where the density may be high. Therefore, we tied its centroid with the main line using certain offsets as mentioned above, and fixed its line-width.

We find that the exclusion of a blended line contribution clearly removes the asymmetry in the observed line profile of Fe XII 195.120 Å, especially in the regions near the footpoints of loops where density is high (cf. figures 4, 5, 6). This shows that the removal of blending can only give the reliable results in the estimation of line-width and Doppler velocity. Single Gaussian fitting may result in an overestimation of these parameters. In the line-width (FWHM measurements), we exclude the thermal component of the width of the Fe XII ($Z = 56$) 195.12 Å spectral line-profile. We find that, for the peak formation temperature of Fe XII ($\log T_e = 6.2$) when the ion equilibrium is established and a level population is formed for a particular emission, the thermal width associated with the chosen line is estimated to be 23.4 mÅ. However, this estimation considers a single ion equilibrium with electrons, which is a most ideal physical scenario that may lead to uncertainties in the measurements. This thermal width is subtracted from the measured total line-width (instrumental width is also

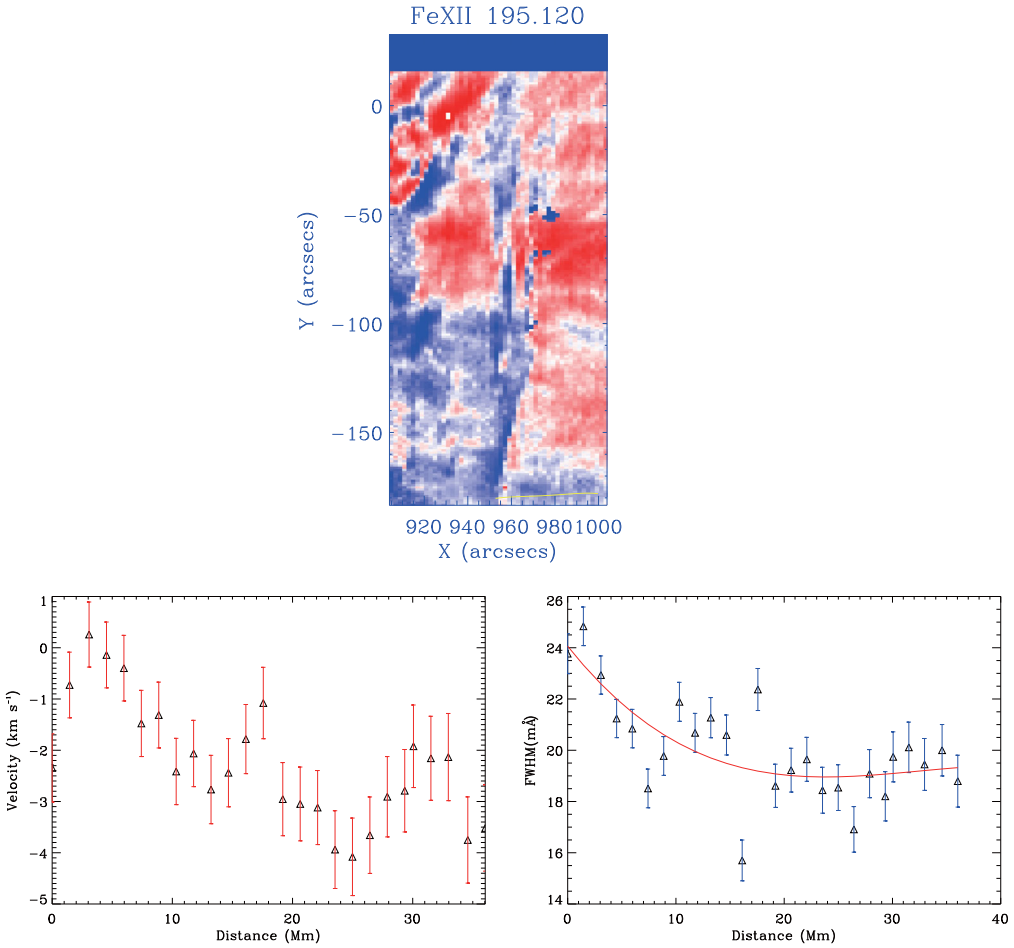

Fig. 2. Top panel: the Fe XII 195.120 Å velocity map shows a blue-shifted coronal funnel. The velocity (bottom-left) and FWHM (bottom-right) profiles w.r.t. height are shown along the path inside the funnel marked in yellow. The zero corresponds to the first point on the chosen path. The third-order polynomial is fitted on the observed data of line-width (red line). Error measurements are obtained from the fitting. (Color online)

already corrected) and therefore the resultant width signifies the line broadening (or narrowing) due to the increment (or decrement) of the non-thermal motions.

Figure 1 displays the intensity map (middle) which shows the lower parts of the off-limb active region loops considered as funnels, as well as the diffused, less intense boundaries. The Doppler map (right) shows that the denser core loops of the active region AR 10940 do have the signature of both blue- and red-shift. The diffused, expanding and less intense boundaries in between exhibit the signature of blue-shift. Both types of region may act as the source region for the flowing plasma as well as the waveguide for transporting wave energy, which can contribute to the formation and acceleration of the nascent solar wind.

The open and expanding regions (figures 2 and 3) are parts of the longer and diffused coronal loops (cf. SOHO/EIT image in figure 1) in the equatorial corona. Therefore, they may serve the role of coronal funnels for the supply of mass and wave energy. The term "open" is used throughout the paper and refers to the magnetic structures that are closed at larger spatial scales. The physical inference is that such loops have a larger length scale and are not in equilibrium. We estimate the approximate hydrostatic scale height of these loops maintained at coronal temperature $\sim$1.0 MK as 80 Mm. However, we select the open funnels as their lower parts up to a height range of 25–30 Mm, which is well below the hydrostatic scale height where these flows are observed. There may be a possibility that such localized funnels are density-structured with less scale height than they would probably have in the non-equilibrium and flows. This description we will discuss in the later part of this paper. Moreover, we select a blue-shifted funnel (figure 7), which is not a part of the curved loop system. However, it lies at the boundary and is most likely associated with less-curved ambient magnetic field lines connecting the higher corona.

The Hinode/EIS has no absolute wavelength for the calibration. Therefore, we have chosen a 2 $\times$ 2 pixel square region in the bottom-right corner of the off-limb region within the field of view (FOV) that is associated with almost

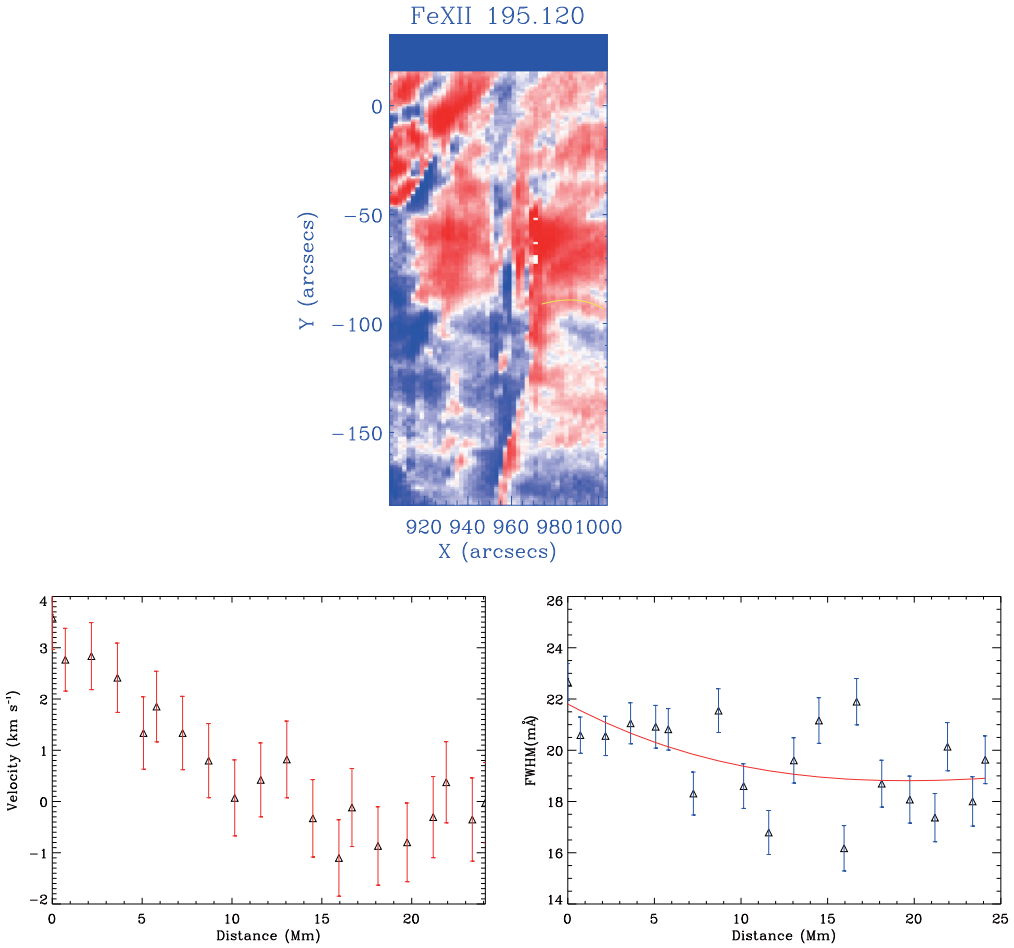

Fig. 3. Top panel: the Fe XII 195.120 Å velocity map shows a red-shifted coronal funnel. The Doppler velocity (bottom-left) and FWHM (bottom-right) profiles w.r.t. height are shown along the path inside the funnel marked by solid yellow line. The zero corresponds to the first point of chosen path. The third-order polynomial is fitted on the observed data of line-width (red-line). Error measurements are obtained from fitting. (Color online)

quiet-Sun without any significant motion. This type of calibration method, choosing the quiet-Sun region, is given in detail by Young, O'Dwyer, and Mason (2012). We derive the integrated spectra, and fit the spectra to derive the absolute reference wavelength, which is 195.119 Å. Assuming this rest wavelength, the velocity profiles and maps have been obtained. The derived averaged central wavelength is very close to the rest wavelength of the chosen Fe XII 195.12 Å spectal line.

Figure 2 shows the variation of the Doppler velocity and line-width along the selected path in the expanding and blue-shifted plasma region (coronal funnel) in the western equatorial corona. The SOHO/EIT image in figure 1 clearly demonstrates that it is a diffused large-scale magnetic structure which is the lower part of the southward loop and its boundary in AR 10940. The Fe XII 195.12 Å line is formed at a typical coronal temperature. When we consider the ion temperature to be equal to the electron temperature in the equilibrium, its thermal width at a given formation temperature will remain constant (cf. Imada et al. 2009), and any change in the FWHM will be attributed to the change in its non-thermal component. Figure 4 represents snapshots of Gaussian fitting after excluding the effect of the blended line on Fe XII 195.120 Å line profiles which show fairly good fittings at (26, 3), (36, 3), and (46, 3) pixels along the chosen path in the coronal funnel. These pixel positions correspond to (950.″96, −180.″90), (976.″92, −178.″90) (998.″88, −178.″90). The dotted line shows the observed line-profile, while the blue solid line displays the fit. The error bars (in blue) are also plotted over these profiles. The bottom left-hand panel of figure 2 displays the variation of the Doppler velocity along the chosen path. It is clear that the blue-shift is almost zero near the footpoint while it increases with height in the funnel. The maximum Doppler velocity associated with the blue-shift is around -4 km s^{-1}. It is to be noted that different regions on the chosen path may be scanned over different time-steps. However, this spatial variation of velocity illustrates the complete scenario of the blue-shifted coronal funnel. The bottom right-hand panel of figure 2 exhibits the variation in

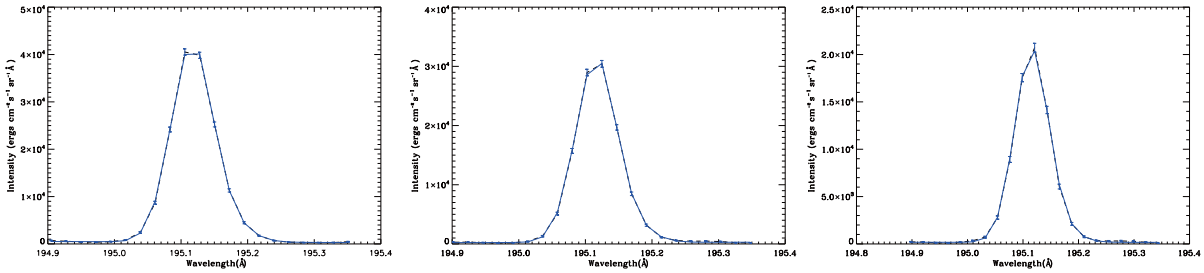

Fig. 4. Some snapshots of Gaussian fitting of the Fe XII 195.120 Å line profile by removing the blending of Fe XII 195.118 Å. Three snapshots show the fits of (23, 2), (36, 4) (47, 4) pixels inside the blue-shifted funnel. These pixel positions correspond to (950″.96, −180″.90), (976″.92, −178″.90) (998″.88, −178″.90). The dotted line shows the observed line-profile, while the blue solid line displays the fit. The error bars in blue are also plotted over these profiles. (Color online)

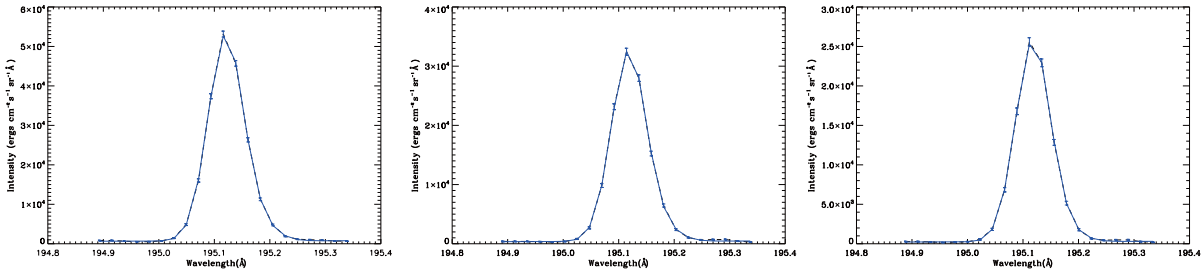

Fig. 5. Same as figure 4 but for the fits of (34, 91), (40, 93), (48, 89) pixels inside the red-shifted funnel. These pixel positions correspond to (972″.92, −91″.90), (980″.91, −89″.90) (1000″.88, −9390″). (Color online)

the thermal width subtracted FWHM of Fe XII 195.120 Å along the same path showing the decreasing trend from 25 to 19 mÅ significantly at higher heights. The third-order polynomial is fitted on the observed data (red line). It also shows that the line-width falls by up to 10 Mm at the lower heights in the funnel, and finally attains a constant value at higher heights.

Figure 3 shows the variation of the Doppler velocity and thermal width subtracted line-width along the selected path in an another expanding and red-shifted plasma region (coronal funnel) in the western equatorial corona, which may possibly be the leg of a higher loop system. Figure 5 represents some snapshots of Gaussian fitting of Fe XII 195.120 Å line profiles which show fairly good fittings at (34, 91), (40, 93), (48, 89) pixels along the chosen path in the red-shifted coronal funnel. These pixel positions correspond to (972″.92, −91″.90), (980″.91, −89″.90), (1000″.88, −93″.90). The dotted line shows the observed line-profile, while the blue solid line displays the fit. The error bars (in blue) are also plotted over these profiles. The bottom left-hand panel of figure 3 displays the variation of the Doppler velocity along the chosen path in the funnel. It is observed that the funnel is asociated with the red-shifted plasma at several heights. However, the Doppler velocity distribution associated with red-shifted regions around zero is attributed to the red-shift being subsided at higher heights. A large uncertainty is however associated with the measurements of Doppler velocities at higher heights in this funnel, which must be taken account of. It should be noted that different regions on the chosen path may be scanned over different time-steps. However, this variation of the velocity shows the overall scenario of the red-shifted parts of the coronal funnel.

The bottom right-hand panel of figure 3 exhibits the variation of the thermal width subtracted FWHM of Fe XII 195.120 Å along the same path, which shows almost constant trend with its slight decrement between 22 to 19 mÅ at higher heights. We find a less negative gradient of the FWHM in this funnel up to 25 Mm height, which is the lower part of a diffused loop system, and consequently treat it as a constant trend.

Figure 7 shows the variation of the Doppler velocity and thermal width subtracted line-width along the selected path in a less intense and blue-shifted boundary of a loop system in the western equatorial corona. Figure 6 represents some snapshots of Gaussian fitting of Fe XII 195.120 Å line profiles which show fairly good fits at (31, 20), (36, 20), (42, 21) pixels along the chosen path. These pixel positions correspond to (966″.93, −162″.90), (976″.92, −162″.90), and (988″.90, −161″.90). The dotted line shows the observed line-profile, while the blue solid line displays the fit. The error bars (in blue) are also plotted over these profiles. The bottom left-hand panel of figure 7 displays the variation of the Doppler velocity along the chosen path.

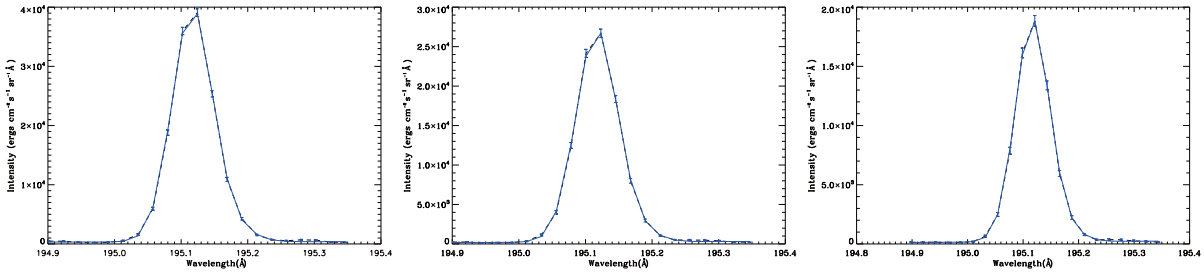

Fig. 6. Some snapshots of Gaussian fitting of Fe XII 195.120 Å line profile. Three snapshots show the fits of (31, 20), (36, 20), (42, 21) pixels respectively inside a path selected along a less intense and blue-shifted boundary of a loop system. These pixel positions correspond to (966.″93, −162.″90), (976.″92, −162.″90), and (988.″90, −161.″90). The dotted line shows the observed line-profile, while the blue solid line displays the fit. The error bars in blue are also plotted over these profiles. (Color online)

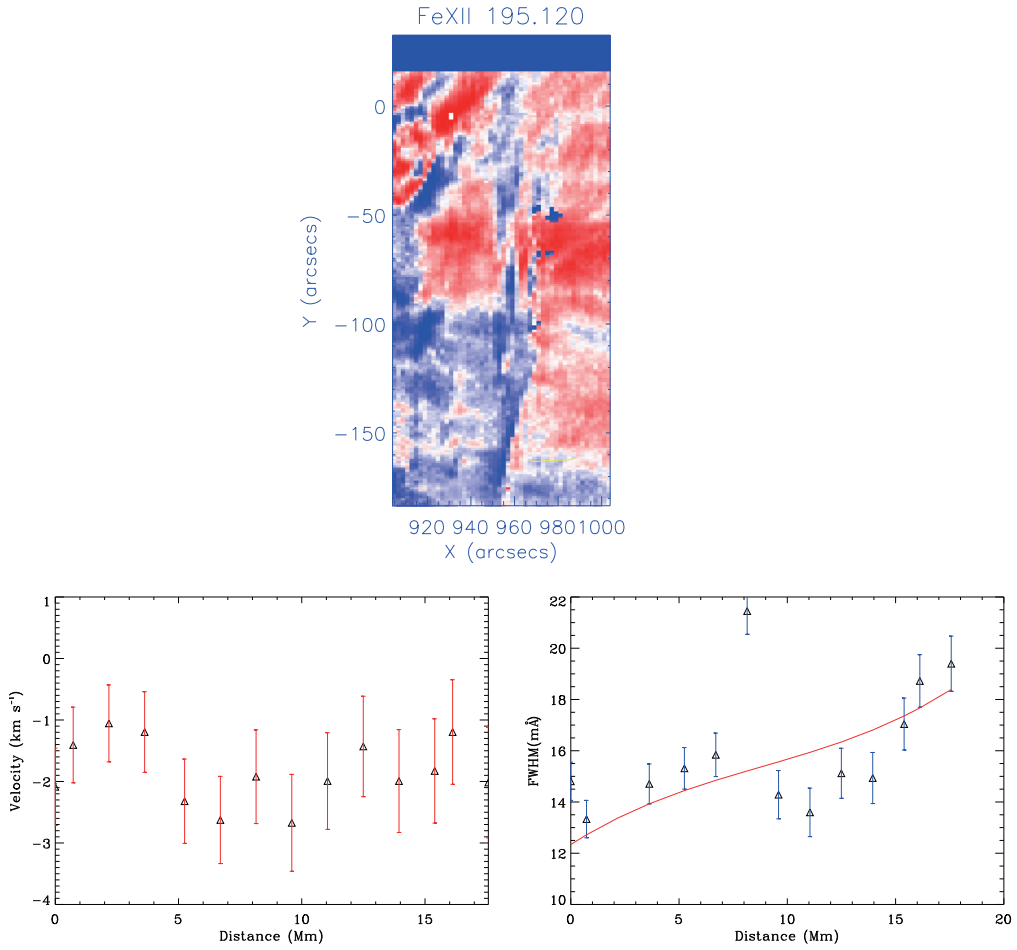

Fig. 7. Top panel: the Fe XII 195.120 Å velocity map showing a path selected along a less intense and blue-shifted boundary of a loop system. The velocity (bottom-left) and FWHM (bottom-right) profiles w.r.t. height along the selected region marked by yellow line are displayed. The zero corressponds to the first point of chosen path. The second-order polynomial is fitted on the observed data of line-width (red-line). Error measurements are obtained from fitting. (Color online)

It is clear that the boundary of the loop system is associated with the blue-shift. Although the measured uncertainties are large, the estimated Doppler velocities and their error bars clearly lie well within the blue-shifted negative velocities. The maximum blue-shift is observed at $\sim$2–3 km s^{-1}. The bottom right-hand panel of figure 7 exhibits the variation in the thermal width subtracted FWHM of Fe XII 195.120 Å along the same path, which shows an increasing trend FWHM from 12 to 19 mÅ in the chosen funnel.

However, the chosen funnels that exhibit blue-shift (figure 2), red-shift (figure 3), and blue-shift (loop

boundary; figure 7) may be associated with the upflows only. The component of flows may depend on the angle of the tube with respect to the equatorial plane. Looking at the SOHO/EIT image (cf. figure 1) of the same region in the western equatorial corona, it is evident that the first funnel (figure 2) is the lower part of southmost lying loop and its boundary seems to be tangled and curved from south-east to north-west with respect to the equatorial plane. Therefore, the plasma may be flowing on a more curved path towards us from its lower to higher part and giving the blue-shifted component in the observed spectral line. The second funnel is the lower part of the diffused coronal loop system lying in the centre of AR 10940 at the western equatorial corona off the limb. The upper part of the selected segment appears to be tilted towards us (see the curvature in figure 3, top panel, as well as the loop system in the SOHO/EIT image in figure 1 shown by the black arrow). This means that the curvature lying away from us and plasma flows on the curved path have Doppler shift component towards the photospheric surface. Therefore, even the plasma in this tube that has the red-shifted signature is basically associated with the upflows from the lower height to higher heights. Although it exhibits the red-shift, yet it may be upflow along the curvature of the tube pointed away from us. The third funnel (figure 7) is evident in EIT and EIS images (figure 1) as a southward boundary and interfaced region of a loop system (less intense and blue-shifted region). The loop system has a curvature and connects from south-east to north-west (cf. SOHO/EIT image). It seems that the boundary along this diffused loop system is associated with the blue-shift, which implies that the plasma is rising along the open field lines and moving towards us and still higher in the ambient corona. Therefore, all the flows that we have observed in the selected tubes may be basically the localized plasma motions that rise from the lower to higher parts of the coronal funnels in the corona.

It is noted that the thermal width subtracted FWHM of Fe XII 195.120 Å in the open and expanding coronal funnel which is the lower part of curved loop-system (out-flowing, figure 2) shows the decreasing trend with height. Therefore, the reduction in the resultant line-width is attributed to the reduction in the non-thermal velocity component caused most likely by the dissipation of Alfvén waves generated at lower heights in this localized flux-tube. In this first funnel, the line-width decreases rapidly up to 10-Mm heights. In general, the spicules or flows can modify the line-width up to 5–10 Mm and can cause the broadening (Doyle et al. 2005). However, we do not consider the low atmospheric spicule and flow contributions in the present case as we are dealing with the spectral line formed at the coronal temperature. Moreover, the thermal component of the line-width is already subtracted in the measurements. Therefore, the line-width decrement up to 10 Mm in height in the first funnel clearly indicates the reduction in the non-thermal component, possibly caused by the localized Alfvén wave dissipation. Harrison, Hood, and Pike (2002) have only observed such a reduction of the line-width in the equatorial corona. However, they found the signature of the dissipation of Alfvén waves in the large-scale loop systems in an equatorial corona. In the present case, it is seen only in the localized coronal funnels instead (figure 2). It is worth mentioning that Wilhelm et al. (2005) could not observe any significant line-width variation in the large-scale equatorial corona. The possible clues of the Alfvén waves and their dissipation in the localized flux-tubes may be entirely episodic. Considering uncertainties in the line-width measurements, it is found that their variation with height in the second funnel is almost constant, with a slight negative gradient with height. At first sight this may exclude any convincing signature of Alfvén wave amplification or dissipation in this localized fluxtube. However, we present the density measurements also in funnels 1, 2, and 3 (cf. figure 8, right-hand panel). The density is measured by the line-intensity ratio of Fe XII 186.88 Å and Fe XII 195.120 Å, which is a density-sensitive line pair (Young et al. 2007). We use the CHIANTI atomic data for its theoretical line ratio as a function of electron density. Using the observed intensity ratio and the CHIANTI atomic data, we estimate the density in equatorial corona in the given field-of-view (figure 8, left-hand panel). It should be noted that the density falls rapidly in this second funnel (blue line) compared to the funnels 1 and 3. Therefore, the high density stratification may cause the abrupt growth of Alfvén waves, which must cause the significant line broadening with height in the second funnel. However, we have a signature of almost constant line-width with slight negative spatial gradient there (cf. the fitted red line in bottom right-hand panel of figure 3). This implies that the Alfvén wave is evolved but dissipation is effectively at work and retains almost a constant line-width. In the case of funnel 1, the gradient of density (red line) is comparatively less, therefore the dissipation is dominant in the amplification of Alfvén waves in the first 10-Mm distance within the tube. Because of continuously decreasing density between 10–35 Mm in the inner corona, the amplification rate of the wave in the stratified atmosphere may become dominant over the dissipation rate. This may further cause an almost constant line-width profile (cf. the fitted red line in bottom right-hand panel of figure 2). Otherwise, the wave must be amplified in such a highly density-stratified magnetic flux tubes. In the case of the third funnel, which is the interfaced boundary region of the diffused loop system, the density decrement is faster at the lower heights (green line in figure 8, right-hand panel).

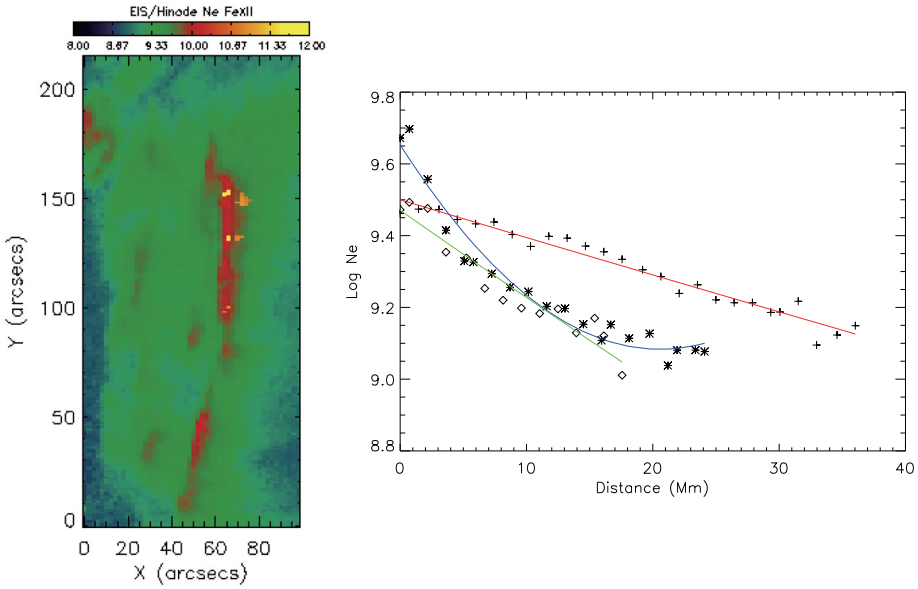

Fig. 8. The left-hand panel displays the density map of the equatorial corona, which shows that density decreases off the limb, while it is high at the footpoints of the various fluxtubes anchored at the limb. The right-hand panel shows the comparison of the decrement of densities in funnel 1 (red), funnel 2 (blue), and funnel 3 (green). These lines are the respective fits to the density w.r.t. height in these funnels. (Color online)

This most likely causes the Alfvén wave growth because the episodic dissipation may be less effective compared to the amplification. However, what factors decide the reduced dissipation is unknown and outwith the scope of this paper. In conclusion, it can be seen that this third funnel chosen in the interfaced and boundary region between these loops exhibits the significantly increasing trend of line-width with height. This most likely indicates that in such less curved and still higher tubes the Alfvén waves may episodically exhibit the signature of growth. In general, these funnels of shorter heights are selected in the present study. If they are maintained at coronal temperatures, the hydrostatic scale height is approximately 80 Mm (for typical 1.0-MK temperature). However, the density measurements (figure 8 right-side panel) show that these funnels are density structured at shorter spatial scales. This may be due to the fact that these localized coronal fluxtubes may be in non-equilbrium states due to the background flows etc., and the longitudinal density structuring may occur in such tubes effectively. Therefore, we find that Alfvén wave growth and dissipation rates are highly dependent on the localized plasma and magnetic fields.

The Alfvén waves can be excited in the expanding and open coronal funnels near their footpoints in the lower atmosphere by photospheric drivers like vortex motions, and then propagate outwards in the form of torsional waves up to the inner coronal heights (Fedun et al. 2011; Musielak et al. 2014). These waves can suffer from the reflection and energy conversion in the chromosphere and transition regions. The sufficient amount of the waves, however, may be transported further into the inner corona. There were magnetic field lines associated with these funnels are smoothly extended to the higher atmosphere, being the parts of the large-scale loop fields (Fedun et al. 2011; Chmielewski et al. 2014; K. Murawski et al. in preparation). Such localized Alfvén waves (either linear or non-linear) cause the line-width broadening at coronal heights as is evident in various observations (Banerjee et al. 1998; O'Shea et al. 2005; Bemporad & Abbo 2012, and references therein), synthesized numerically (Chmielewski et al. 2013, 2014), and demonstrated by simple analytical models (Dwivedi & Srivastava 2006; Srivastava & Dwivedi 2007). The line-width increment with height in the solar corona is attributed to the amplification of Alfvén waves, while its reduction or flattening demonstrates their dissipation of Alfvén waves (Banerjee et al. 1998; O'Shea et al. 2005).

As far as the equatorial corona is concerned, our observations show the line-width variations with height in the localized coronal funnels. However, we do not find any signature of its increment in the funnels which are the lower parts of the curved coronal loops. We either find the reduction in the line-width (funnel 1) or its constant trend (funnel 2) with height. It should be noted that we start this measurement slightly above the limb in order to avoid its effects, and do observe the line-width variations at the coronal temperatures. Therefore, it is likely that we do not constrain exactly the footpoints of the coronal funnels, and instead we do estimate the parameters from a certain height above their footpoints. Therefore, we conjecture that the

Alfvén waves that are excited near the footpoints of these tubes are further dissipated still in the lower heights within these tubes. It caused the reduction in the non-thermal component and finally the reduction in the observed line-width. There may be the dissipation may occur due to classical collisional dissipative agents, e.g., viscosity and resistivity (see Dwivedi & Srivastava 2006). However, these classical dissipative agents may not be significant at the coronal temperatures (Spitzer 1962). Therefore, the Alfvén wave should grow up to the inner coronal heights and cause the increment in the line-width (Banerjee et al. 1998; O'Shea et al. 2005). However, that is not what we observe here in the localized coronal funnels. Therefore, it is quite possible that the Alfvén wave, after its excitation above the photosphere, is dissipated due to the mode conversion (cf. Zaqarashvili et al. 2007; Srivastava & Dwivedi 2010) in the lower solar atmosphere. Therefore, the Alfvén wave is dissipated at lower heights and its energy flux (as well as velocity amplitude) is continuously reduced up to the inner corona. This may either reduce the non-thermal component of line-width (funnel 1) or can subside its increment (funnel 2). Another possibility is that if such waves are excited due to the rotation of the footpoints or due to the excitation of MHD pulses near the footpoint in such funnels associated with curved loops (e.g., funnels 1 and 2), there exists a third that the magnetic curvatures, and the inhomogeneity in plasma properties as well as the magnetic field of the loop system to which they are associated, will further cause the phase-mixing. As a result, waves will be dissipated at shorter spatio-temporal scales through the ambient medium. This also depends on the nature and properties of the exciters, e.g., pulse, rotation of footpoint etc. (cf. Nakariakov et al. 1997; Del Zanna et al. 2005; and references cited therein). Therefore, the above-mentioned mechanisms may be possible candidates in the reduction of the non-thermal component of the observed spectral line due to Alfvén wave dissipation, which further causes the reduction in FWHM as observed in the coronal part of the localized atmosphere as shown in figures 3 and 5. However, such excitation and dissipation of the Alfvén waves in the localized fluxtubes may be episodic and depends on the localized drivers excited within the tube as well as the local plasma and magnetic field conditions there (Fedun et al. 2011).

It is interesting to note that the line-width along the boundary or interfaced region (less intense and blue-shifted) between the loop arches exhibits the increasing trend. This provides no clues to Alfvén wave dissipation. The density decrement is greater at lower heights, which may cause the dominance of growth of Alfvén waves compared to their dissipation. This is most likely that above discussed dissipative mechanisms may not be efficiently at work in this region. On contrary, we have the signature of Alfvén wave growth in this funnel as the non-thermal component increases with height. This means that the Alfvén wave, once excited in the localized magnetic flux-tubes, is strongly affected by the local plasma and magnetic field properties. The tube associated with the interfaced boundary region may expand as an ambient magnetic field still higher in the corona with less curvature.

In conclusion, we obtain the signature of Alfvén wave dissipation in the equatorial corona especially in the localized coronal funnels or flux-tubes which are associated with the more curved coronal loops (e.g., funnels 1 and 2). Such wave dissipation may heat the plasma at the inner coronal heights, which may further expand into the higher atmosphere, contributing to the formation of the nascent solar wind. It is noteworthy that in the first funnel we find the sharp decrement of the line-width below 10 Mm height, which may be the height within the funnel where solar wind is energized (Tu et al. 2005). Therefore, the dissipation of Alfvén waves may impart energy in the lower parts of the funnel to heat and expand the nascent wind further contributing to its formation at higher coronal heights.

Acknowledgments

We thank the referee for their most valuable suggestions which substantially improved our manuscript. We acknowledge the Hinode/EIS observations for this study. Hinode is a Japanese mission developed and launched by ISAS/JAXA, with NAOJ as domestic partner and NASA and UKSA as international partners. It is operated by these agencies in co-operation with ESA and NSC (Norway). BND is supported by the organizers of the Hinode-7. AKS acknowledges Shobhna for her encouragement, and P. Kayshap for discussions on Hinode/EIS analyses.

References

Banerjee, D., Teriaca, L., Doyle, J. G., & Wilhelm, K. 1998, A&A, 339, 208
Bemporad, A., & Abbo, L. 2012, ApJ, 751, 110
Bradshaw, S. J., Aulanier, G., & Del Zanna, G. 2011, ApJ, 743, 66
Chmielewski, P., Srivastava, A. K., Murawski, K., & Musielak, Z. E. 2013, MNRAS, 428, 40
Chmielewski, P., Srivastava, A. K., Murawski, K., & Musielak, Z. E. 2014, Acta Phys. Pol. A, 125, 158
Culhane, J. L., Doschek, G. A., Watanabe, T., et al. 2006, Proc. SPIE, 6266
Del Zanna, L., Schaekens, E., & Velli, M. 2005, A&A, 431, 1095
Doyle, J. G., Giannikakis, J., Xia, L. D., & Madjarska, M. S. 2005, A&A, 431, 17
Dwivedi, B. N., & Srivastava, A. K. 2006, Sol. Phys., 237, 143
Fedun, V., Verth, G., Jess, D. B., & Erdélyi, R. 2011, ApJ, 740, L46
Habbal, S. R., Woo, R., Fineschi, S., O'Neal, R., Kohl, J., Noci, G., & Korendyke, C. 1997, ApJ, 489, L103

Harra, L. K., Sakao, T., Mandrini, C. H., Hara, H., Imada, S., Young, P. R., van Driel-Gesztelyi, L., & Baker, D. 2008, ApJ, 676, L147
Harrison, R. A., Hood, A. W., & Pike, C. D. 2002, A&A, 392, 319
Imada, S., Hara, H., & Watanabe, T. 2009, ApJ, 705, L208
Jian, L. K., Russell, C. T., Luhmann, J. G., Strangeway, R. J., Leisner, J. S., & Galvin, A. B. 2009, ApJ, 701, L105
Marsch, E., Zhou, G.-Q., He, J.-S., & Tu, C.-Y. 2006, A&A, 457, 699
McIntosh, S. W., de Pontieu, B., Carlsson, M., Hansteen, V., Boerner, P., & Goossens, M. 2011, Nature, 475, 477
Musielak, Z. E., Murawski, K., & Srivastava, A. K. 2014, BAAS, 223, 118.06
Nakariakov, V. M., Roberts, B., & Murawski, K. 1997, Sol. Phys., 175, 93
Ofman, L., & Davila, J. M. 1995, J. Geophys. Res., 100, 23413
O'Shea, E., Banerjee, D., & Doyle, J. G. 2005, A&A, 436, L35
Sakao, T., et al. 2007, Science, 318, 1585
Spitzer, L. 1962, Physics of Fully Ionized Gases, 2nd ed. (New York: Interscience)
Srivastava, A. K., & Dwivedi, B. N. 2007, J. Astrophys. Astron., 28, 1
Srivastava, A. K., & Dwivedi, B. N. 2010, MNRAS, 405, 2317
Srivastava, A. K., Konkol, P., Murawski, K., Dwivedi, B. N., & Mohan, A. 2014, Sol. Phys., submitted (doi:10.1007/s11207-014-0584-9)
Subramanian, S., Madjarska, M. S., & Doyle, J. G. 2010, A&A, 516, A50
Suzuki, T. K., & Inutsuka, S. 2005, ApJ, 632, L49
Tian, H., McIntosh, S. W., Wang, T., Ofman, L., De Pontieu, B., Innes, D. E., & Peter, H. 2012, ApJ, 759, 144
Tripathi, D., Mason, H. E., Del Zanna, G., & Bradshaw, S. 2012, ApJ, 754, L4
Tu, C.-Y., & Marsch, E. 1997, Sol. Phys., 171, 363
Tu, C.-Y., Zhou, C., Marsch, E., Xia, L.-D., Zhao, L., Wang, J.-X., & Wilhelm, K. 2005, Science, 308, 519
Wilhelm, K., Fludra, A., Teriaca, L., Harrison, R. A., Dwivedi, B. N., & Pike, C. D. 2005, A&A, 435, 733
Young, P. R., et al. 2007, PASJ, 59, S857
Young, P. R., O'Dwyer, B., & Mason, H. E. 2012, ApJ, 744, 14
Young, P. R., Watanabe, T., Hara, H., & Mariska, J. T. 2009, A&A, 495, 587
Zaqarashvili, T. V., Oliver, R., Ballester, J. L., & Shergelashvili, B. M. 2007, A&A, 470, 815